DOI https://doi.org/10.5281/zenodo.10049652#103

TWIST, 2024, Vol. 19, Issue 1, pp. 377-381

TWIST

Journal homepage: www.twistjournal.net

First Principal Study for Concentration Profile of Mn Doped $ZnSnAs_2$

Anuj Kumar*
[1]- Department of Physics, School of Applied Sciences, Shri Venkateshwara University,
NH-24, Gajraula, 244236, Uttar Pradesh, India
[2]- Department of Physics, Mahamaya Government Degree College,
NH-74, Bijnor, 246747, Uttar Pradesh, India
[**Corresponding author*]

Aman Kumar
Department of Physics, Keral Verma Subharti College of Science, Swami Vivekanand Subharti University,
NH-58, Meerut, 250005, Uttar Pradesh, India

Sandeep Kumar Pundir
Department of Physics, Lucknow University,
University Road, Lucknow, 226007, Uttar Pradesh, India

Nempal Singh
Department of Physics, School of Applied Sciences, Shri Venkateshwara University,
NH-24, Gajraula, 244236, Uttar Pradesh, India

Abstract
We report a detailed first principal spin-polarized density functional calculation for an electronic profile of Mn-doped $ZnSnAs_2$ by using full potential linearized augmented plane wave (FP-LAPW) and Tran-Blaha's modified Becke-Johnson (TB-mBJ) functional approach. Mn doping in $ZnSnAs_2$ takes at Sn site and induces large magnetic moment. Mn replaces Sn by using a selective Mn doping mechanism which is fourth nearest neighbouring Sn Sites. Where Mn shows a 3d transition metal element with an oxidation state +4. We find the half-metallic and high-spin ferromagnetic state in Mn-doped $ZnSnAs_2$ and it may be highly useful for spintronics applications. We also observed with increasing Mn concentration in $ZnSnAs_2$, bandgap increases in one magnetic state (down spin) with an average rate of 0.07 eV per percentage concentration of Mn while the magnetic momentum of the unit cell remains unchanged.

Keywords
Supercell, Degenerate Semiconductor, Band Gap, Ferromagnetism

INTRODUCTION

In the last few decades, chalcopyrite semiconductors have gained significant attraction in the scientific community. Several experimental and theoretical studies on such compounds have been done in the last few decades. This type of compound has huge possibilities to be used in Light Emitting Diode (LED), Infra-red (IR) sensors, IR LEDs, optical paramagnetic oscillators, and spintronics [1-5]. The non-magnetic properties of chalcopyrite semiconductors XYZ (I-III−VI2 and II−IV−V2) can be reversed by doping of a high spin d-state material [6]. N. Uchitomi and co-workers revealed; that when Mn-doped ZnSnAs2 thin films are grown on an InP substrate they show phase transitions from ferromagnetic to paramagnetic at a Curie temperature (CT) near room temperature [7-8]. Later Shiro Hidaka varied Mn doping concentrations on the same thin films, the variation in Mn concentrations ranged from 0.5% to 25% investigated the corresponding variation in CT of the material and found 2-4% variation in CT [1-2, 6, 8-9]. In literature, the first principal investigation, at 300 K shows ZnSnAs2 has band gap values ranging from 0.30 eV - 0.75 eV [9-12]. We also found that ZnSnAs2 transforms from non-magnetic to magnetic when doped by Mn [ref]. Mn-doped ZnSnAs2 exhibits

anti-ferromagnetism by interactions with Mn II−MnII site pairs and shows ferromagnetism by MnII−MnIV and MnIV−MnIV site pairs interaction [6]. So herein, among these sites, it will be a useful MnIV−MnIV site for ferromagnetic interaction [13]. It is typical for the Replacement of Sn atoms by Mn in Mn-doped ZnSnAs2 since Zn sites have a natural tendency for Mn to adopt a divalent state and turn into a lower energy anti-ferromagnetic state [6, 14-15]. The replacement of Sn atoms by Mn introduced spin-doped material which enables carrier-induced ferromagnetism, replaced by the fourth nearest neighbouring Sn atom [16]. All these studies give useful information of Mn-doped ZnSnAs2 but it has not been clarified and is still under debate about the deformation in electronic structures and the physical origin of magnetic states in chalcopyrite. Kohn-Sham equation gives the numerical values for energy and density in the form of integer numbers with discontinuous derivatives. Usually, a large value of discontinuous derivative does not allow the calculation for the closest electron system (close atoms) which is very important in electronic structure theory and density functional theory (DFT). In explanation to include discontinuity derivative, we substituted exchange potential with TB-mBJ potential [19]. For determining the band gap and band diagram of the material, we used TB-mBJ functional instead of the local density approximation (LDA) and GGA [19]. This situation motivates us to study the electronic and magnetic properties using FP-LAPW with local orbitals in order to gain a better understanding of material properties.

In this work we have studied the space groups as part of the structural properties of Mn-doped ZnSnAs2, to know about the variation in electronic parameters of the Mn-doped material we have performed a systematic detailed study of the bandgap profile. A comparative study of band gap variation with concentration performed by TB-mBJ and Perdew-Burke-Ernzerhof 's generalized gradient approximation (GGA-PBE) method. These Sturdy were carried out for a dopant concentration of Mn 9.0% or above.

METHOD OF CALCULATIONS

We have used FP-LAPW method in WIEN2k package to investigate the first principal calculations. Further the electronic exchange-correlation refined using GGA-PBE method. The wave function of charge density and potential in the interstitial region is increased up to l_{max} = 10 in each computational and energy cut-off of $R_{MT}.K_{max}$ = 7.0, respectively. Where R_{MT} denotes the smallest atomic sphere radius, and K_{max} denotes the magnitude of the maximal K-vector in the plane wave expansion, the smaller value of R_{MT} needs more plane waves. The quantity of k-points is being augmented to enhance the precision of electronic structure computations. The mesh of 5x5x5 k points were utilized to satisfied the whole Brillouin zones. A supercell of base material was created by Wein2k programme and this supercell was utilised for further calculations. We may dope Mn in the supercells in six types by changing unit cell dimensions and number of Mn atom/unit cell. These types are followings;

(i) When dope Mn=0 atom, the supercell consists 16 atoms 4Zn, 4Sn, and 8As with dimension axbxc, where, a, b, and c are lattice parameters.

(ii) When doped Mn=1 atom, the supercell consists 128 atoms, 32Zn, 31Sn, 1Mn and 64As with dimension 2ax2bx2c.

(iii) When doped Mn=1 atom, the supercell consists 64 atoms 16Zn, 15Sn, 1Mn and 32As with dimension 2ax2bxc.

(iv) When doped Mn=1 atom, the supercell consists 32 atoms 8Zn, 7Sn, 1Mn and 16As with dimension 2axbxc.

(v) When doped Mn=1 atom, the supercell consists 16 atoms 4Zn, 3Sn, 1Mn and 8As with dimension axbxc.

(vi) When doped Mn=1 atom, the supercell consists 16 atoms 4Zn, 2Sn, 2Mn and 8As with dimension axbxc arranged simple tetragonal. The weight percentage of Mn concentration in I-VI supercells considered as 0%, 0.51%, 1.02%, 1.11%, 4.32% and 9.09%, respectively.

RESULTS AND DISCUSSION

Electronic Structures

Stable electronic structures analysis by Murnaghan's state equation. We have use input structure parameters a=5.85A, c= 11.70A, and u = 0.23, and the atomic position of Zn (0,0,0) with R_{MT} = 2.25, Sn (0.25,0.75,0.50) with RMT= 2.39, As (u = 0.23, 0.225, 0.125), (where u is the internal distortion parameter) with R_{MT} = 2.24 respectively [3] and optimize the same by GGA-PBE. another input structure parameter of the same atoms with Mn (0.5,0.5,0) doping with optimize by GGA- PBE where Mn replacing with Sn atoms. Resultant internal distortion parameter (u) is shown in the Table-1, these results are clearly showing the bond length between Zn-As and Sn-As are not same and supercell not have symmetric around x-axis.

Table 1 Calculated internal distortion parameter (u), normalized tetragonal parameter (c/2a), and magnetic momentum of Unit cell (μB)

Supercell	u	c/2a	μB	Space Group
Supercell-I	0.222[a], 0.231[b], 0.225[c], 0.240[d]	1.03[a],0.99[b],1.00[c]	0.00a	122-I-42d
Supercell-II	0.224[a]	1.04[a]	2.99[a], 3.00[b]	81-P-4
Supercell-III	0.221[a]	0.99[a], 0.98[e]	3.02[a], 3.10[b]	81-P-4
Supercell-IV	0.222[a]	0.98[a]	2.99[a]	81-P-4
Supercell-V	0.221[a]	0.98[a]	2.99[a]	81-P-4
Supercell-VI	0.223[a]	1.02[a]	3.00[a], 4.00[c]	82-I-4

[a]This Work, [b][5],[c][6],[d][8],[e][23]

To change the doping concentration, the lattice parameter needs to be extents twice from the original lattice parameter. Modified lattice parameter is used to calculate the tetragonal distortion parameter (c/2a), and as shown in Table-1. These results show, doping has only a minor effect on the structure of the compound, thus we get clear information that there will be no special effect on the optical and mechanical properties of the compound. The obtained values of lattices parameter and coordinates are in good agreement with the reported theoretical and experimental data. The lattice structure of maximum dopant supercell $Zn_4Mn_2Sn_2As_8$ and its respective primitive Brillouin zone are shown in Fig-1 (a) and Fig-1 (b), respectively. ZnSnAs2 has space group no. 122 (I-42d) which exists body-centred tetragonal unit cell with inversion 4-fold, 2-fold with mirror symmetry, and 16 symmetrical operations. Mn replaces fourth nearest neighbouring Sn (0.5,0.5,0) and we observed change in space group 122 to 81, which has a primitive tetragonal unit cell with 4-fold symmetry and 4 symmetrical operations. Subsequent, doping of two Mn atom at the site of Sn (0.5,0.5,0) and (0.75,0.25,0) space group change to 82 and we have a body-cantered which one is show in Fig-1 (a) tetragonal unit cell, space group 82 have 4-fold symmetry and 4 symmetrical operations. These significant changes in material structure may be due to atomic interaction developed by Mn dopant.

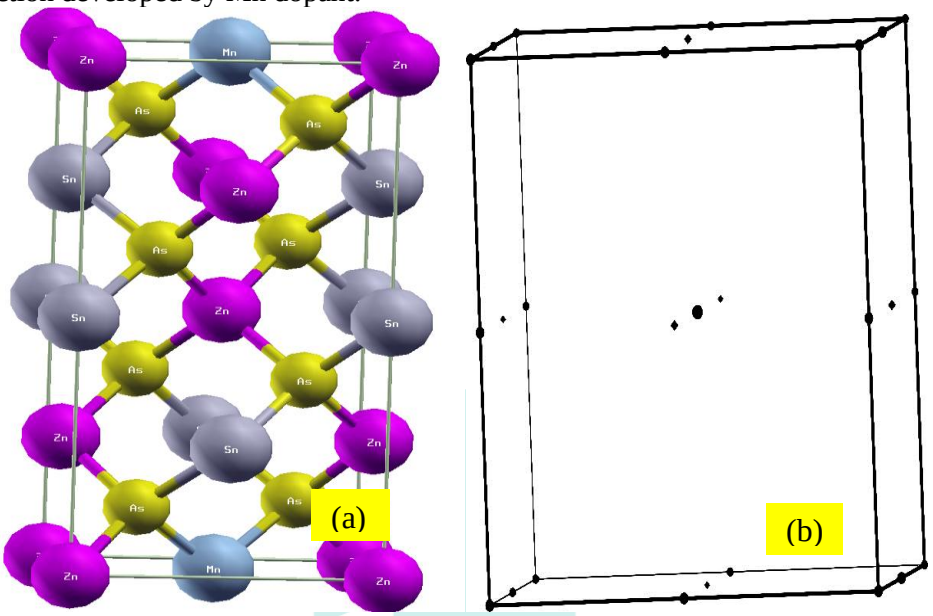

Fig. 1 (a) Crystal structure of maximum dopant supercell $ZnSn_{(1-x)}Mn_xAs_2$ for x=0.5 (b) respective primitive Brillouin zone

Electronic and magnetic properties

Self-consistent field calculations (SCF) were carried out by TB-mBJ and gave the Fermi energy value of 0.33 eV of the compounds. For the high-symmetrical band diagram, we have chosen Z, Γ, X, M, and R as k-points for energy range -4.0 eV to 4.0 eV. The calculated electronic band structure of each supercell is highly symmetric in the first Brillouin zone about the Γ k-point. The total and partial Density of State (PDOS) of the $ZnSnAs_2$ are shown in Fig-2, respectively.

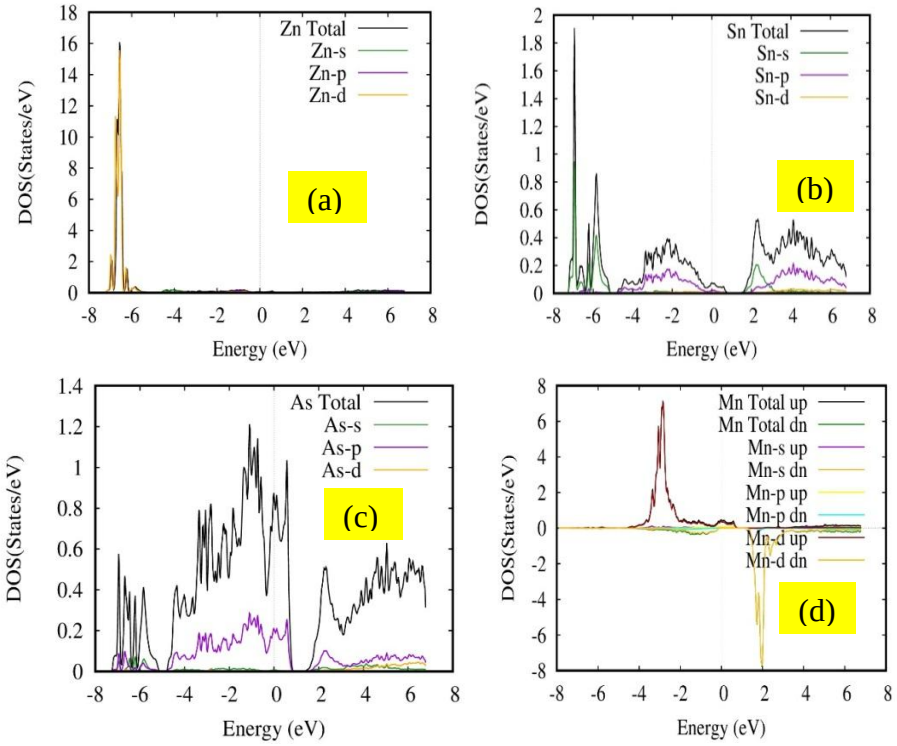

Fig. 2 PDOS of (a) Zn, (b) Sn, (c) As, and (d) Mn (up and down State) of $ZnSn_{(1-x)}Mn_xAs_2$ for x=0.25

It is observed from the Partial DOS calculations the contribution in valence band (VB) formation is mainly due to the p-state of As and Zn atoms, and d state of Zn atoms, whereas the conduction band formation is due to s, p-states of Sn and As Atoms. As we doped Mn in the material, d-state of Mn start contributes significantly in both VB of up-spin and CB of down-spin. In case of pure $ZnSnAs_2$ Fermi Level found to be between CB and VB as depicted. The schematic plot of band diagram of Mn dopant supercells is reported in Fig-5. It is also observed form the band diagram, the $ZnSnAs_2$ shows a direct bandgap at Γ k-point for both up and down spin, and band gap equal to 0.75 eV, with Fermi level at 0.33 eV which lie approximately between CB and VB. It is very close match with the experimental values given in the literature [8]. Mn dopant supercell also shows a direct band gap semiconductor at Γ k-point in both states. It is also observed from the band diagram host atom and dopant Mn atom have strong hybridization between electronic states. In the case of down state, on increasing the Mn concentration in material the system leads to the elevation in CB and lowering of VB. While in the case of up state as we increase the concentration of Mn, the CB bottom level goes up, and the VB top level also goes up. As a result, the material's band gap increases in the down state while decreasing in up-state. This is also observed from the up states band diagram, the fermi level is appearing in valance band and therefore behave like degenerate semiconductor so there is no bandgap observed. A comparative concentration profile of Mn doped $ZnSnAs_2$ by three different approaches is shown in Fig-4. This shows the band gap increases at an average rate of 0.07 eV as we increase Mn concentration in the material as calculated by TB-mBJ method. On the other hand, GGA+U approach calculation with SGGA profile shows the bandgap increase with an average rate of 0.02 eV, and GGA+PEB approach shows an average rate of 0.05 eV. In Fig 4, curve obtained from TB-mBJ method shows the first half (ranges from 0% to 4%) has bandgap increase rate equal to 0.08 eV, and the second half (ranges 4% to 9%) has increased rate equal to 0.06 eV, respectively. The magnetic moment given in Table-1 is calculated from the Mulliken population analysis. The magnetic moment of all cells is approximately fixed and does not change with doping concentrations and is equal to 3.0 μB. It is expected from chalcopyrite materials when doped with +4 oxidation state atom, results a maximum magnetic moment of 3 μB observed [6]. Such as in case of Mn doping in $ZnSnAs_2$ we find a magnetic moment is 3.63 μB at 1.56% concentration doping at temperature of 5K [15]. 5% and 7% Mn concentration doped thin film of $ZnSnAs_2$, also shows magnetic moment of 0.87 μB and 2.75 μB, respectively [2]. The reported value and experimental data are in very good agreement with each other.

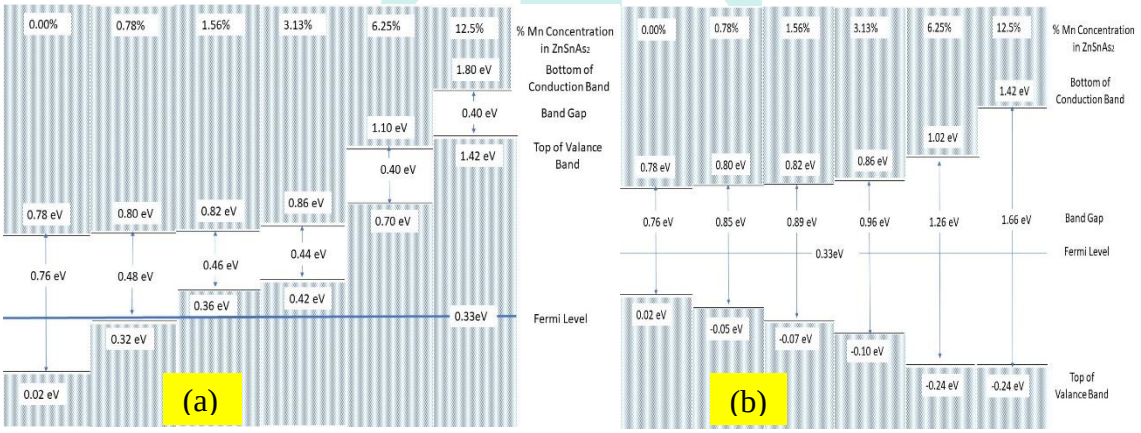

Fig. 3 The schematic plot of band diagram of Mn Doped $ZnSnAs_2$ (a) Up Spin (b) Down Spin

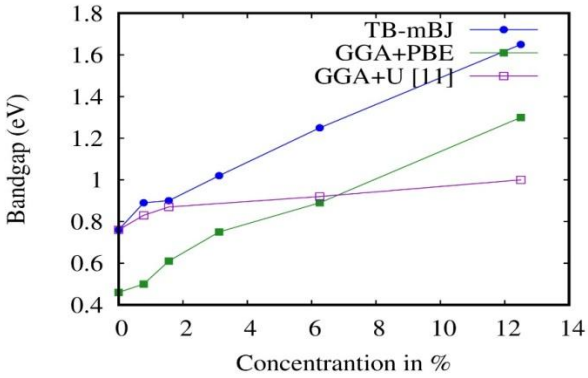

Fig. 4 The Bandgap concentration profile of Mn doping in $ZnSnAs_2$

CONCLUSION

We have studied the electronic profile of Mn-doped $ZnSnAs_2$ by first principal calculation. The calculation shows the pure $ZnSnAs_2$ is a direct band gap with a value 0.75 eV non-magnetic semiconductor, and coincide with experimental data. High spin magnetic moment of 3.0 μB resulted by Mn doping at Sn atom fourth site. The results show an up-state fermi level overlap with the valance band and a down-state fermi level found between both the bands. So, in the up state, the semiconductor behaves like a degenerated semiconductor, whereas in the down state as a normal semiconductor. Because of these, this material may be very useful for spintronic applications, commercial fabrication of mass storage devices and optical ferromagnetic devices, etc.

FUNDING INFORMATION
This work is supported by Government of Uttar Pradesh (India) Grant number; Letter No. 41/2022/1554-sattar-5-2022/001-70-5099-539-2020. One of the author Anuj Kumar has received research support from Mahamaya Government Degree College, Sherkot, Bijnor, Uttar Pradesh (India).

DECLARATION OF CONFLICT
Conflict of interest/Competing interests - All the authors declare that they have no conflict of interest.

ACKNOWLEDGMENTS
This work was partly supported by the State Government of Uttar Pradesh (India) with Letter No. 41/2022/1554-sattar-5-2022/001-70-5099-539-2020.

REFERENCES

1. Uchitomi, N., Oomae, H., Toyota, H., Yamagami, K., Kambayashi, T.: Magnetic, electrical and structural properties of annealed ferromagnetic (zn, sn) as2: Mn thin films on inp substrates: comparison with undoped znsnas2. In: EPJ Web of Conferences, vol. 75, p. 03007 (2014). EDP Sciences
2. Oomae, H., Asubar, J.T., Jinbo, Y., Uchitomi, N.: Anomalous hall effect and magnetoresistance in mn-doped znsnas2 epitaxial film on inp substrates. Japanese Journal of Applied Physics 50(1S2), 01–12 (2011)
3. Uchitomi, N., Hidaka, S., Saito, S., Asubar, J.T., Toyota, H.: Magnetic phase change in mn-doped znsnas2 thin films depending on mn concentration. Journal of Applied Physics 123(16) (2018)
4. Uchitomi, N., Oomae, H., Asubar, J.T., Endo, H., Jinbo, Y.: Room-temperature ferromagnetism in (zn, mn, sn) as2 thin films applicable to inp-based spintronic devices. Japanese Journal of Applied Physics 50(5S2), 05–02 (2011)
5. Hayashi, K., Uchitomi, N., Yamagami, K., Suzuki, A., Yoshizawa, H., Asubar, J.T., Happo, N., Hosokawa, S.: Large as sublattice distortion in sphalerite znsnas2 thin films revealed by x-ray fluorescence holography. Journal of Applied Physics 119(12) (2016)
6. Bouhani-Benziane, H., Sahnoun, O., Sahnoun, M., Driz, M., Daul, C.: Magnetic exchange interactions in mn doped znsnas2 chalcopyrite. Journal of Magnetism and Magnetic Materials 396, 345–349 (2015)
7. Kizaki, H., Morikawa, Y.: First-principles study of znsnas2-based dilute magnetic semiconductors. Japanese Journal of Applied Physics 57(2), 020306 (2018)
8. Liu, H., Zhao, B., Yu, Y., He, Z., Xiao, J., Huang, W., Zhu, S., Chen, B., Xie, L.: Theoretical investigations on elastic, thermal and lattice dynamic properties of chalcopyrite znsnx2 (x= p, as, sb) under pressure and temperature: The firstprinciples calculation. International Journal of Modern Physics B 32(30), 1850329 (2018)
9. Asubar, J.T., Jinbo, Y., Uchitomi, N.: Mbe growth of mn-doped znsnas2 thin films. Journal of crystal growth 311(3), 929–932 (2009)
10. Khan, K., Gaur, A., Ahuja, U., Soni, A., Sahariya, J.: Density functional investigations to study effect of m=(ge, sn) doping on opto-electronic response of znsi (1–x) mxp2. Optik 208, 164570 (2020)
11. Mecheri, B., Meradji, H., Ghemid, S., Bendjeddou, H., Boukhtouta, M.: Structural and electronic properties of znsias 2, znsnas 2, and their mixed crystals znsi 1–x sn x as 2. Semiconductors 55, 146–153 (2021)
12. Jafarova, V., Huseynova, S., Orudzhev, G., Uchitomi, N., Wakita, K., Mamedov, N.: Ab-initio study of ferromagnetism in mn-doped znsnas2. physica status solidi (c) 12(6), 668–671 (2015)
13. Ishikawa, M., Nakayama, T.: First-principles study of doping properties in znsnas2. physica status solidi (c) 12(6), 814–817 (2015)
14. Choi, S., Cha, G.-B., Hong, S.C., Cho, S., Kim, Y., Ketterson, J., Jeong, S.-Y., Yi, G.-C.: Room-temperature ferromagnetism in chalcopyrite mn-doped znsnas2 single crystals. Solid State Communications 122(3-4), 165–167 (2002)
15. Blaha, P., Schwarz, K., Tran, F., Laskowski, R., Madsen, G.K., Marks, L.D.: Wien2k: An apw+ lo program for calculating the properties of solids. The Journal of chemical physics 152(7) (2020)
16. Mori-S´anchez, P., Cohen, A.J.: The derivative discontinuity of the exchange– correlation functional. Physical Chemistry Chemical Physics 16(28), 14378–14387 (2014)
17. Kokalj, A.: Computer graphics and graphical user interfaces as tools in simulations of matter at the atomic scale. Computational Materials Science 28(2), 155–168 (2003)
18. Soni, A., Gaur, A., Khan, K., Sahariya, J.: Electronic, structural and optical features for ternary znsnas2 compound: a first principle's density functional investigation. Materials Today: Proceedings 19, 564–567 (2019)
19. Kumar, A., Jharwal, S., Prajapati, B., Kumar, M., Singh, V., Singh, R.P.: Theoretical investigations on electronic and optical properties of half heusler alloy, fenbsb for opto-electronic applications. Optical and Quantum Electronics 54(11), 717 (2022)
20. Hidaka, S., Toyota, H., Uchitomi, N.: Antiferromagnetic-ferromagnetic phase transition in (zn, sn, mn) as2 epitaxial thin films. Applied Physics Letters 110(13) (2017)
21. Munro, J.M., Latimer, K., Horton, M.K., Dwaraknath, S., Persson, K.A.: An improved symmetry-based approach to reciprocal space path selection in band structure calculations. npj Computational Materials 6(1), 112 (2020)
22. Sreeparvathy, P., Kanchana, V., Vaitheeswaran, G.: Thermoelectric properties of zinc based pnictide semiconductors. Journal of Applied Physics 119(8) (2016)
23. Choi, S., Choi, J., Hong, S.C., Cho, S., Kim, Y., Ketterson, J.B.: Mn-doped zngeas2 and znsnas2 single crystals: Growth and electrical and magnetic properties. JOURNAL-KOREAN PHYSICAL SOCIETY 42, 739–741 (2003).